Journal of Power Sources 196 (2011) 2661–2668

Contents lists available at ScienceDirect

Journal of Power Sources

journal homepage: www.elsevier.com/locate/jpowsour

Performance improvement of proton exchange membrane fuel cell by using annular shaped geometry

I. Khazaee*, M. Ghazikhani

Engineering Faculty, Mechanical Engineering Department, Ferdowsi University of Mashhad, Mashhad, P.O. Box 9177948944-1111, Iran

ARTICLE INFO

Article history:
Received 22 September 2010
Received in revised form 23 October 2010
Accepted 7 November 2010
Available online 13 November 2010

Keywords:
PEM fuel cell
Annular shaped
Numerical modeling
Current density
Polarization curve
Gas concentration

ABSTRACT

A complete three-dimensional and single phase CFD model for a different geometry of proton exchange membrane (PEM) fuel cell is used to investigate the effect of using different connections between bipolar plate and gas diffusion layer on the performances, current density and gas concentration. The proposed model is a full cell model, which includes all the parts of the PEM fuel cell, flow channels, gas diffusion electrodes, catalyst layers and the membrane. Coupled transport and electrochemical kinetics equations are solved in a single domain; therefore no interfacial boundary condition is required at the internal boundaries between cell components.

This computational fluid dynamics code is used as the direct problem solver, which is used to simulate the three-dimensional mass, momentum and species transport phenomena as well as the electron- and proton-transfer process taking place in a PEMFC that cannot be investigated experimentally. The results show that the predicted polarization curves by using this model are in good agreement with the experimental results. Also the results show that by increasing the number of connection between GDL and bipolar plate the performance of the fuel cell enhances.

1. Introduction

The polymer exchange membrane fuel cell (PEMFC) is considered to be the most promising candidate for electric vehicles by virtue of its high power density, zero pollution, low operating temperature, quick start-up capability and long lifetime. PEMFC can also be used in distributed power systems, submarines, and aerospace applications [1].

The single-cell PEMFC consists of a carbon plate, a gas diffusion layer (GDL), a catalyst layer, for each of the anode and the cathode sides, as well as a PEM membrane at the center.

Flow channel geometry is of critical importance for the performance of fuel cells containing proton exchange membranes (PEM) but is of less concern for solid oxide fuel cells (SOFC). The reactants, as well as the products, are transported to and from the cell through flow channels. Flow field configurations, including parallel, serpentine, interdigitated, and other combined versions, have been developed.

The losses of voltage in the fuel cell dominate over different current density ranges. For low current densities; the activation over-potential is dominant. For high current densities, which are of particular interest for vehicle applications because of higher power density; the mass transfer limitations dominates the losses. For moderate current densities, the ohmic drop across the polymer membrane dominates. Moreover, for high current densities, water starts to exist in liquid form leading to a two-phase transport of reactants to reaction site, which is an additional transport phenomenon of PEM Fuel Cell operation.

Berning and Djilali [2] examined the effect of the porosity and thickness of gas diffusion layer in straight channel with three-dimensional model. These PEMFC numerical analysis models contributed to the optimization of component design and operation condition, and to the examination of issues included in present cell. However, these studies calculated internal phenomena in short straight gas channel and one serpentine channel or in small cell, and there are very few researches that evaluated various component shapes of actual size cell under considering realistic calculation time and calculation resource.

Chiang and Chu [3] investigated the effects of transport components on the transport phenomena and performance of PEM fuel cells by using a three-dimensional model. The impacts of channel aspect ratio (AR) and GDL thickness were examined. It was found that a flat channel with a small AR or a thin GDL generates more current at low cell voltage due to the merits of better reactant gas transport and liquid water delivery.

Wang et al. [4] developed a two-dimensional numerical model to study the two-phase flow transport in the air cathode of a PEMFC. In this paper, the model encompassed both single and two-phase regimes corresponding to low and high current

* Corresponding author. Tel.: +98 511 8796580; fax: +98 511 8763304.
E-mail address: imankhazaee@yahoo.com (I. Khazaee).

0378-7753/$ – see front matter © 2010 Elsevier B.V. All rights reserved.
doi:10.1016/j.jpowsour.2010.11.052

Nomenclature

A	superficial electrode area (m^2)
C	molar concentration ($mol\ m^{-3}$)
D	species diffusivity ($m^2\ s^{-1}$)
I	current density ($A\ m^{-2}$)
i_0	reference current density ($A\ cm^{-2}$)
U	inlet velocity ($m\ s^{-1}$)
j	transfer current density ($A\ m^{-3}$)
$\vec{u}$	velocity vector ($m\ s^{-1}$)
p	pressure (Pa)
S	stoichiometric ratio
T	temperature (K)

Greek letters

η	overpotential (V)
ρ	density ($kg\ m^{-3}$)
ε	porosity
σ	ionic conductivity ($S\ m^{-1}$)
ϕ	phase potential (V)
ν	volumetric flow rate ($m^3\ s^{-1}$)
ξ	water content of the membrane
μ	viscosity ($kg\ m\ s^{-1}$)
α	transfer coefficient for the reaction

densities and was capable of predicting the transition between the two regimes.

Kuo et al. [5] performed numerical simulations to evaluate the convective heat transfer performance and velocity flow characteristics of the gas flow channel design to enhance the performance of proton exchange membrane fuel cells (PEMFCs). Their study has simulated low Reynolds number laminar flow in the gas flow channel of a PEMFC. The heat transfer performance and enhanced gas flow velocity characteristics of four different channel geometries have been considered, namely a conventional straight gas flow channel and a gas flow channel with the three novel periodic patterns geometries. The results indicated that, compared to the conventional gas flow channel, the novel gas flow channels proposed in this study provide a significantly improved convective heat transfer performance and a higher gas flow velocity and, hence, an improved catalysis reaction performance in the catalyst layer.

Yi and Nguyen [6] proposed an along the channel model for evaluating the effects of various design and parameters on the performance of a PEMFC. The results show that the humidification of the anode gas is required to enhance the conductivity of the membrane, and the liquid injection and higher humidification temperature can improve the cell performance by introducing more water into the anode. It is noted that the mass transport processes in the presence of liquid water are not considered in these two-dimensional models.

Um and Wang [7] used a three-dimensional model to study the effects an interdigitated flow field. The model accounted for mass transport, electrochemical kinetics, species profiles and current density distribution within the cell. Interdigitated flow fields result in forced convection of gases, which aids in liquid water removal at the cathode. This would help improve performance at high current densities when transport limitations due to excessive water production are expected. The model shows that there is little to no difference at low to medium current densities between an interdigitated flow field and a conventional flow field.

In this work a three-dimensional and single phase CFD model for annular-shaped geometry of proton exchange membrane (PEM) fuel cell is presented to investigate the effect of using different connections between bipolar plate and gas diffusion layer on the performances, current density and gas concentration. The objective of the current work is to show using a different geometry of the fuel cell and the effect of increasing the connections between bipolar plate and gas diffusion layer that it may be of interest to engineers attempting to develop the optimization of a PEMFC and to researchers interested in the flow modification aspects of the PEMFC performance enhancement.

2. Numerical model

The cathode electrochemical reactions produce a large amount of liquid water at low operating voltages. If the liquid water is not properly removed and accumulates in the pores of the porous layers, it restricts the oxygen transport to the gas diffusion layer and the catalyst layer, thereby reducing the electrochemical reaction rate.

The numerical model for the fuel cell used here includes the anode flow channels, anode gas diffusion layer, anode catalyst layer, proton exchange membrane, cathode catalyst layer, cathode gas diffusion layer, and cathode flow channels. Miniature annular fuel cells with dimensions of $D = 4.8$ mm and $L = 12$ mm are considered in this investigation. The gas diffusion layer is 0.3 mm thick, the catalyst layer is 0.01 mm thick, and the proton exchange membrane is 0.05 mm thick.

The geometrical relations in this study are for six different connections between GDL and bipolar plate.

The physical problem considered in this paper is the three-dimensional cell model of the PEMFC system as shown in Fig. 1.

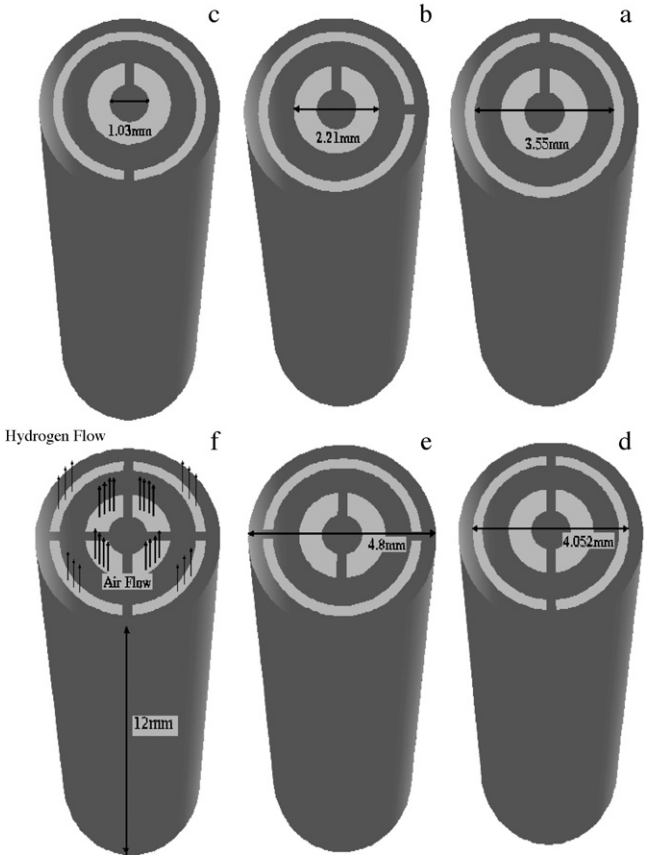

Fig. 1. Computational domain and schematic of annular PEMFC with (a) one connection (1), (b) one connection (2), (c) one connection (3), (d) two connection (1), (e) two connection (2) and (f) four connection.

Table 1
Source terms.

	S_v (momentum)	S_k (species)	S_ϕ (phase potential)	S_h (energy)
Gas channels	0	0	0	0
Backing layers	$-\frac{\mu}{k}\varepsilon^2\vec{\mu}$	0	0	0
Catalyst layers	$-\frac{\mu}{k}\varepsilon^2\vec{\mu}$	$-\frac{J_a}{2F}\frac{\rho}{\varepsilon_m\varepsilon_{mc}}$: anode H_2 $\frac{J_c}{2F}\frac{\rho}{\varepsilon_m\varepsilon_{mc}}$: cathode O_2 $-\frac{J_c}{F}\left(\frac{1}{2}+n_d\right)\frac{\rho}{\varepsilon_m\varepsilon_{mc}}$: cathode H_2O $-\frac{n_d}{F}J_a\frac{\rho}{\varepsilon_m\varepsilon_{mc}}$: anode H_2O	j	$\frac{\lvert j_c\rvert}{2F}T\lvert\Delta s\rvert+\lvert j_c\eta_c\rvert$ for cathode 0 for anode
Membrane	$-\frac{\mu}{k}\varepsilon^2\vec{\mu}$	0	0	$\frac{j^2}{k_{mem}}$

The proposed model does not require any internal boundary conditions between the components of PEM Fuel Cell system. The different physical properties and transport parameters are incorporated into a single set of governing equations using a single domain formulation. The model aims to study the electrochemical kinetics, current distribution, reactant flow fields and multi-component transport of oxidizer and fuel streams in a multi-dimensional domain. The assumptions made in developing the model are as follows:

- Ideal gas mixtures.
- Incompressible and laminar flow because low flow velocities and low fuel utilization.
- Isotropic and homogeneous porous electrodes, catalyst layers and membrane.
- Negligible ohmic resistance at porous electrodes and current collectors.

The model assumes that the system is steady; the inlet reactants are ideal gases; the flow is laminar; and the porous layers such as the diffusion layer, catalyst layer and PEM are isotropic. The model includes continuity, momentum and species equations for gaseous species, liquid water transport equations in the channels, gas diffusion layers, and catalyst layers, water transport equation in the membrane, electron and proton transport equations. The Bulter–Volmer equation was used to describe electrochemical reactions in the catalyst layers.

The conservation equations of mass, momentum, energy, species and charge are as follows:

$$\frac{\partial(\rho\varepsilon)}{\partial t}+\nabla\cdot(\varepsilon\rho\vec{u})=0 \tag{1}$$

$$\frac{\partial(\rho\varepsilon\vec{u})}{\partial t}+\nabla\cdot(\varepsilon\rho\vec{u}\vec{u})=-\varepsilon\nabla p+\nabla\cdot(\varepsilon\mu\nabla\vec{u})+S_u \tag{2}$$

$$\frac{\partial(\rho\vec{u}(E+p))}{\partial t}+\nabla\cdot((E+p)\rho\vec{u}\vec{u}) = \nabla\cdot\left(\lambda_{eff}\nabla T-\sum_k h_k J_k+(\tau_{eff}\cdot\vec{u})\right)+S_h \tag{3}$$

$$\frac{\partial(\varepsilon X_k)}{\partial t}+\nabla\cdot(\varepsilon\vec{u}X_k)=\nabla\cdot(D_k^{eff}\nabla X_k)+S_k \tag{4}$$

$$\nabla\cdot(\sigma_g^{eff}\nabla\phi_e)+S_\phi=0 \tag{5}$$

where $\vec{u}$, X_k, h_k, τ_{eff}, λ_{eff} and ϕ_e denotes intrinsic velocity vector, molar fraction of kth species, enthalpy of species k, effective stress tensor which can be ignored due to the low velocity of laminar gas flow, effective thermal conductivity in a porous material consisting of the electrode solid matrix and gas and electrolyte phase potential, respectively. The corresponding source terms (S_k, S_ϕ, S_u, S_h) treating the electrochemical reactions and porous media are presented in Table 1.

$$\lambda_{eff}=\varepsilon\lambda_f+(1-\varepsilon)\lambda_s \tag{6}$$

where λ_s is the thermal conductivity of the electrode solid matrix and λ_f is the thermal conductivity of the gas, which can be expressed as a function of temperature:

$$\lambda_f=a_0+a_1T+a_2T^2+a_3T^3 \tag{7}$$

It is of benefit to further explain the corresponding diffusivities of the governing equations. The diffusivities for species concentration equations and ionic conductivity for membrane phase potential equation are modified using Bruggman correlation to account for porous electrodes, which can be expressed as:

$$D_k^{eff}=\varepsilon_m^{1.5}D_k \tag{8}$$

$$\sigma_e^{eff}=\varepsilon_m^{1.5}\sigma_e \tag{9}$$

It is worth further explaining the mole fraction of oxygen appearing in Eq. (3) because oxygen is a gaseous species in the cathode flow channel and gas-diffusion electrode but becomes a species dissolved in the electrolyte in the catalyst layer and membrane regions. Our definition is given by

$$X_k=\begin{cases}C_k^g/C_{tot} & \text{in gas}\\ C_k^e/C_{tot} & \text{in electrode}\end{cases} \tag{10}$$

where C_k is the molar concentration of species k and superscripts g and e denote the gas and the electrolyte phases, respectively. Thus, X_k is a true mole fraction in the gas phase but is a pseudo mole fraction when species k is in the dissolved form. In addition, there is a discontinuity in the value of X_k at the interface between the gas-diffusion electrode and the catalyst layer due to the following thermodynamic relation:

$$C_k^{e,sat}=\frac{RT}{H}C_k^g \tag{11}$$

where H is the Henry's law constant equal to 2×10^5 atm cm^3 mol^{-1} for oxygen in the membrane.

Either generation or consumption of chemical species k and the creation of electric current occurs only in the active catalyst layers where electrochemical reactions take place. The S_k and S_ϕ terms are therefore related to the transfer current between the solid matrix and the membrane phase inside each of the catalyst layers. These transfer currents at anode and cathode can be expressed as follows:

$$j_a=aj_{0,a}^{ref}\left(\frac{X_{H_2}}{X_{H_2,ref}}\right)^{1/2}\left(\frac{\alpha_a+\alpha_c}{RT}\cdot F\cdot\eta\right) \tag{12}$$

$$j_c=-aj_{0,c}^{ref}\left(\frac{X_{O_2}}{X_{O_2,ref}}\right)^{1/2}\left(-\frac{\alpha_c\cdot F}{RT}\cdot\eta\right) \tag{13}$$

The above kinetics expressions are derived from the general Bulter–Volmer equation based on the facts that the anode exhibits

fast electrokinetics and hence a low surface overpotential to justify a linear kinetic rate equation, and that the cathode has relatively slow kinetics to be adequately described by the Tafel equation. In Eqs. (9) and (10), the surface overpotential, $h(x, y)$, is defined as

$$\eta(x, y) = \phi_s - \phi_e - V_{oc} \tag{14}$$

where ϕ_s and ϕ_e stand for the potentials of the electronically conductive solid matrix and electrolyte, respectively, at the electrode electrolyte interface. V_{oc} is the reference open-circuit potential of an electrode. V_{oc} is the reference open-circuit potential of an electrode. It is equal to zero on the anode but is a function of temperature on the cathode namely

$$V_{oc} = 0.0025T + 0.2329 \tag{15}$$

where T is in Kelvin and V_{oc} is in Volts. Notice that V_{oc} is not the true open-circuit potential of an electrode, which would then depend upon reactant concentrations according to the Nernst equation.

Eq. (9), which is a rewritten form of the Nernst equation, precisely describes the effect of decreasing transfer current under hydrogen dilution. The dependence of the cathodic exchange current density on temperature can be fitted as

$$\frac{i_0(T)}{i_0(353\,\mathrm{K})} = \exp(0.014189(T - 353)) \tag{16}$$

The species diffusivity, D_k, varies in different subregions of the PEMFC depending on the specific physical phase of component k. In flow channels and porous electrodes, species k exists in the gaseous phase, and thus the diffusion coefficient takes the value in gas, whereas species k is dissolved in the membrane phase within the catalyst layers and the membrane, and thus takes the value corresponding to dissolved species, which is usually a few orders of magnitude lower than that in gas. In addition, the diffusion coefficient is a function of temperature and pressure.

$$D(T) = D_0 \left(\frac{T}{T_0}\right)^{3/2} \left(\frac{p_0}{p}\right) \tag{17}$$

The proton conductivity in the membrane phase has been correlated as

$$\sigma_e(T) = 100 \exp\left[1268\left(\frac{1}{303} - \frac{1}{T}\right)\right](0.005139\xi - 0.00326) \tag{18}$$

where the water content in the membrane, ξ, depends on the water activity, a, according to the following fit of the experimental data:

$$\xi = \begin{cases} 0.043 + 17.18a - 39.85a^2 + 36a^3 & 0 < a \le 1 \\ 14 + 1.4(a - 1) & 1 \le a \le 3 \end{cases} \tag{19}$$

The water activity is in turn calculated by

$$a = \frac{X_{H_2O} p}{p_{sat}} \tag{20}$$

where the saturation pressure of water vapor can be computed from the following empirical equation:

$$\ln(p^{sat}) = 70.43464 - \frac{7362.698}{T} + 0.006952T - 9\ln(T) \tag{21}$$

In a fuel cell system, the inlet flow rates are generally expressed as stoichiometric ratios of inlet streams based on a reference current density. The stoichiometric ratios inlet streams are given by the following equations:

$$S^{anode} = C_{H_2} \upsilon^{anode} \frac{2F}{I_{ref} A} \tag{22}$$

$$S^{cathode} = C_{O_2} \upsilon^{cathode} \frac{4F}{I_{ref} A} \tag{23}$$

Water transport through the polymer electrolyte membrane has been investigated by several researchers in different aspects.

Table 2
Electrochemical and transport properties.

Description	Unit	Value
Anode reference exchange current density	$A\,m^{-3}$	1.5E9
Cathode reference exchange current density	$A\,m^{-3}$	4,000,000
Anode transfer coefficient		2
Cathode transfer coefficient		2
Faraday constant	$C\,mol^{-1}$	96,487
H_2 diffusivity	$m^2\,s^{-1}$	3E−5
O_2 diffusivity	$m^2\,s^{-1}$	3E−5
H_2O diffusivity at anode	$m^2\,s^{-1}$	3E−5
H_2O diffusivity at cathode	$m^2\,s^{-1}$	3E−5
Anode backing layer porosity		0.5
Cathode backing layer porosity		0.5
Permeability of anode backing layer	m^2	E−12
Permeability of cathode backing layer	m^2	E−l2
Equivalent weight of membrane	$kg\,mol^{-1}$	1.1

Table 3
Operational parameters.

Description	Unit	Value
Reference average current density	$A\,cm^{-2}$	1.0
Anode inlet velocity	$m\,s^{-1}$	0.5
Cathode inlet velocity	$m\,s^{-1}$	1
Anode inlet pressure	atm	1
Cathode inlet pressure	atm	1
Cell temperature	°C	70
Anode inlet molar concentration		
Hydrogen	$mol\,m^{-3}$	35.667
Oxygen	$mol\,m^{-3}$	0
Water vapor	$mol\,m^{-3}$	16.121
Cathode inlet molar concentration		
Hydrogen	$mol\,m^{-3}$	0
Oxygen	$mol\,m^{-3}$	7.51
Water vapor	$mol\,m^{-3}$	16.121

Most interesting studies in this area includes the determination of water diffusion coefficient [8] and water drag coefficient [9] by Zawodzinski et al. and investigating the diffusion of water in Nafion membranes by Motupally et al. [10].

The electro-osmotic drag coefficient is defined as the number of water molecules transported by each hydrogen proton H^+. The electro-osmotic drag coefficient can be expressed with the following equation:

$$n_d = \frac{2.5\xi}{22} \tag{24}$$

The diffusion coefficient of water in polymer membrane is also highly dependent on the water content of the membrane. The relation is given as:

$$D_w^m = \left\{ \begin{array}{ll} 3.1 \times 10^{-7}\xi(\exp(0.28\xi) - 1)\exp(-2346/T) & 0 < \xi < 3 \\ 4.17 \times 10^{-8}\xi(1 + 161\exp(-\xi))\exp(-2346/T) & \text{otherwise} \end{array} \right\} \tag{25}$$

Once the electrolyte phase potential is determined in the membrane, the local current density along the axial direction can be calculated as follows:

$$I(y) = -\sigma_e^{eff} \left.\frac{\partial \phi_e}{\partial x}\right|_{x=\text{I.F.}} \tag{26}$$

where I.F. means the interface between the membrane and cathode catalyst layer. The average current density is then determined by

$$I_{avg} = \frac{1}{L}\int_0^L I(y)\,dy \tag{27}$$

where L is the cell length.

There are natural boundary conditions of zero-flux prescribed everywhere other than the inlet and outlets of the flow channels.

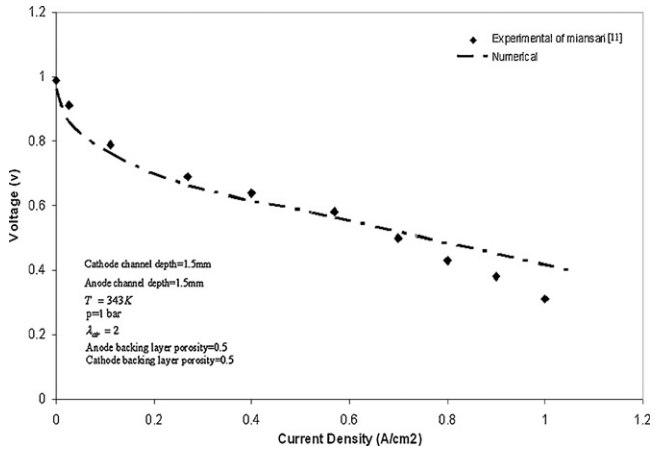

Fig. 2. Comparison between results of this paper and results of Miansari et al. [11].

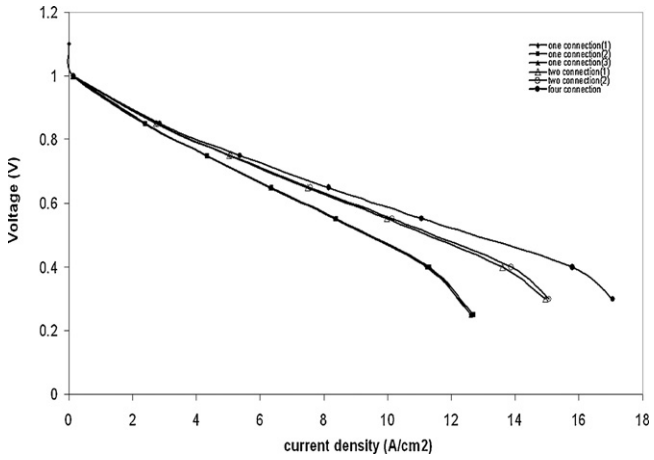

Fig. 3. Variation of cell performance with (a) one connection (1), (b) one connection (2), (c) one connection (3), (d) two connection (1), (e) two connection (2) and (f) four connection.

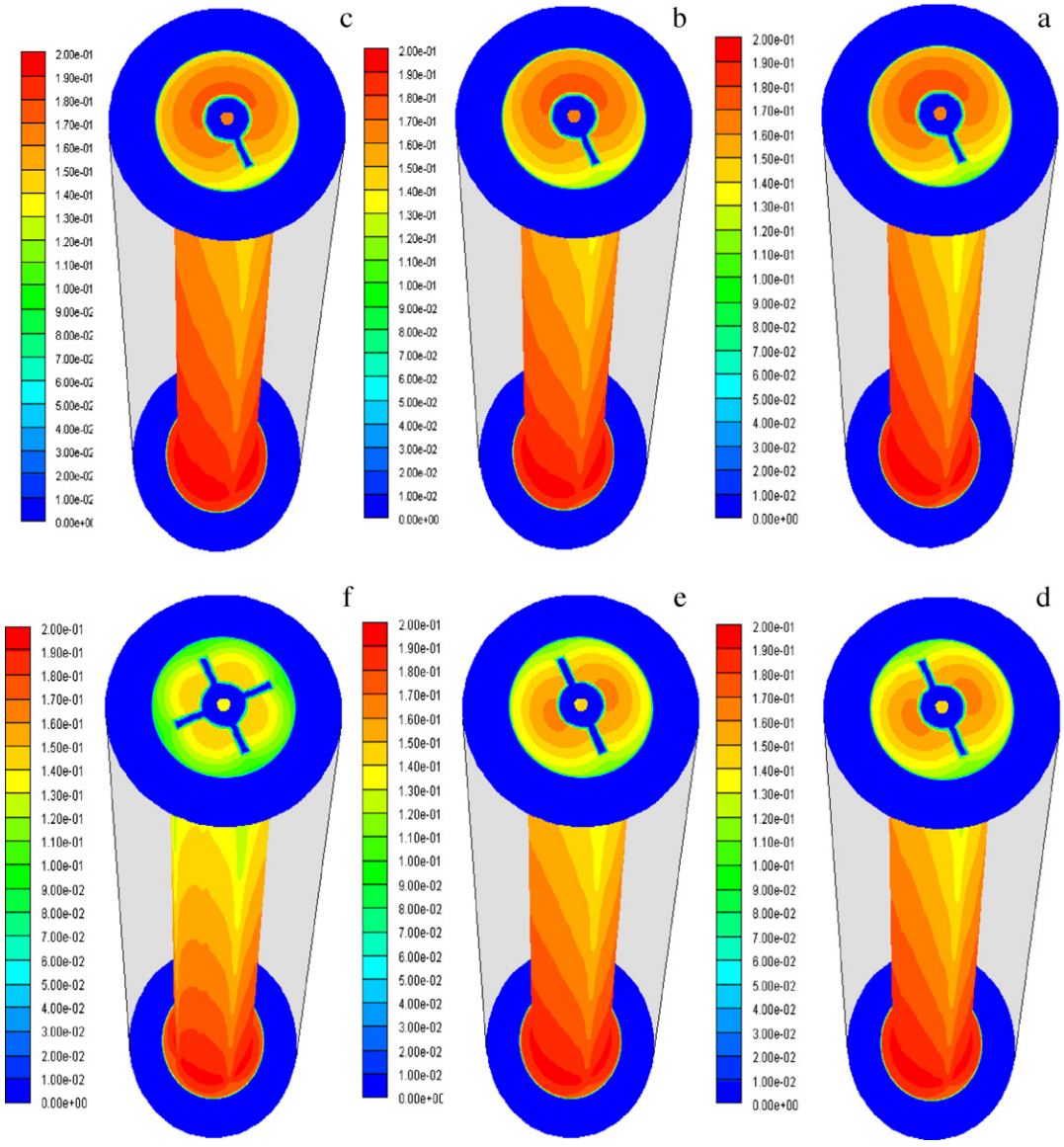

Fig. 4. Oxygen mass fraction distribution in the cathode side channel at $V = 0.4$ V with (a) one connection (1), (b) one connection (2), (c) one connection (3), (d) two connection (1), (e) two connection (2) and (f) four connection.

The boundary conditions prescribed at the inlets of the gas channels are:

$u_{in}^{anode} = u_a^0$	$u_{in}^{cathode} = u_c^0$
$C_{H_2}^{anode,in} = C_{H_2}^0$	$C_{O_2}^{cathode,in} = C_{O_2}^0$
$C_{H_2O}^{anode,in} = C_{H_2O}^{0,a}$	$C_{H_2O}^{cathode,in} = C_{H_2O}^{0,c}$

A mesh with 543,426 nodes was found to provide required spatial resolution for different channel geometry. The solution is considered to be converged when the difference between successive iterations is less than 10^{-7} for all variables.

The electrochemical and transport parameters used in these simulations are summarized in Table 2, and the operational parameters are presented in Table 3.

3. Results and discussion

In order to show that the program in this study can handle the cell performance of a PEMFC, we apply the present method to solve the whole of a PEMFC as described in Miansari et al. [11] paper. The physical parameters and properties of the fuel cell are listed in Fig. 2. The mesh employed for the comparison with the reference was $241 \times 74 \times 25$. The steady-state solution is obtained by the numerical procedure as mentioned in the previous section. As shown in Fig. 2, the result of the present predictions of the polarization curve agreeing fairly closely with Miansari et al. [11] gives one confidence in the use of the present program.

Fig. 3 shows the polarization curves of the annular-shaped fuel cell for different channels geometry with six connections between bipolar plate and gas diffusion layer to investigate the influence of the internal flow modification on the overall cell performance. It shows in Fig. 3 that the effect of the number of connections between GDL and bipolar plate on the cell performance is significant at low operating voltage conditions. However, at high operating voltage conditions, the influence of the connections on the *I–V* curve is negligibly small. It is also observed that the cell performance is increased as the number of connections between GDL and bipolar plate increases but for one connection conditions the effect of

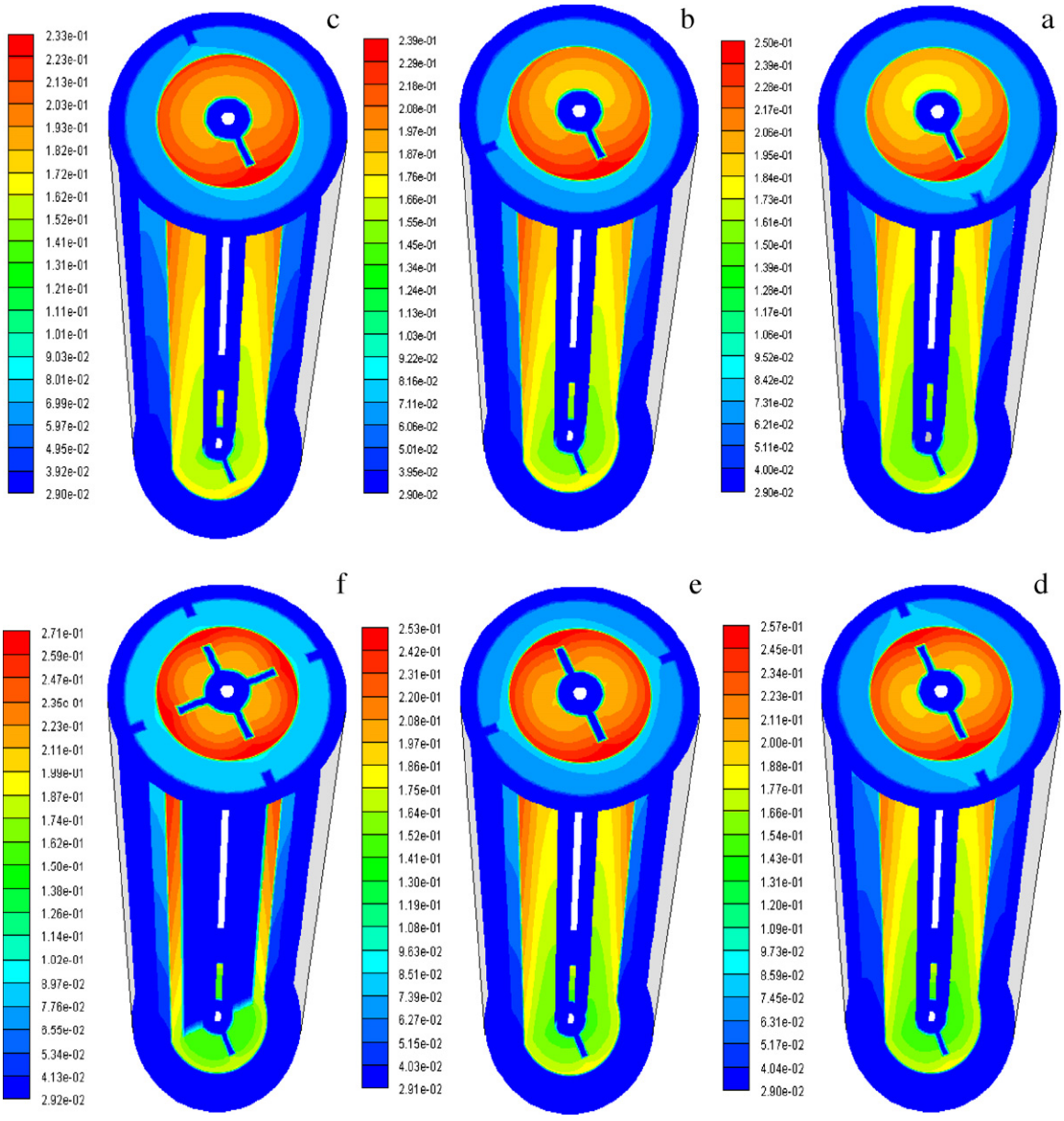

Fig. 5. Water mole fraction distribution in the cell at $V = 0.4$ V with (a) one connection (1), (b) one connection (2), (c) one connection (3), (d) two connection (1), (e) two connection (2) and (f) four connection.

changing the location of connection on cell performance is negligibly small. This is due to the increase of concentration gradient with increasing the number of gas channels, which in turn, results in a higher mass transfer to the catalyst layer. Therefore, a larger current density takes place.

Fig. 4 shows the mass fraction contours of oxygen, respectively, obtained at $V = 0.4$ V for six different conditions of connection between GDL and bipolar plate in the cathode side. As shown in Fig. 4 the oxygen mass fraction decreases along the channel due to the consumption of oxygen species within the catalyst layer. Results show that the mass fraction of the oxygen decreases as the number of connection increases but it is clear that the reduction of oxygen for one connection (1) condition is more than one connection (2), (3). However, as shown in this figure, the reduction of oxygen concentration along the channel is not instantly sensed at the GDL/CL boundary because the concentration of oxygen at the catalyst layer is balanced by the oxygen that is being consumed and the amount of oxygen that diffuses towards the catalyst layer, driven by the concentration gradient. As a result, a more uniform profile for the oxygen concentration is read when the number of connection between GDL and bipolar plate increases. Also the decrease in mass fraction of the oxygen along the cathode side is higher than for the hydrogen in anode side due to the smaller diffusivity of the oxygen.

The water molar fraction distribution in the cell is shown in Fig. 5 at $V = 0.4$ V for six different connections between GDL and bipolar plate. As shown in Fig. 5 water molar fraction increases along the channel due to (i) the water production by oxygen consumption at the catalyst layer and (ii) the net water transfer from the anode side through the membrane toward the cathode side. However, the

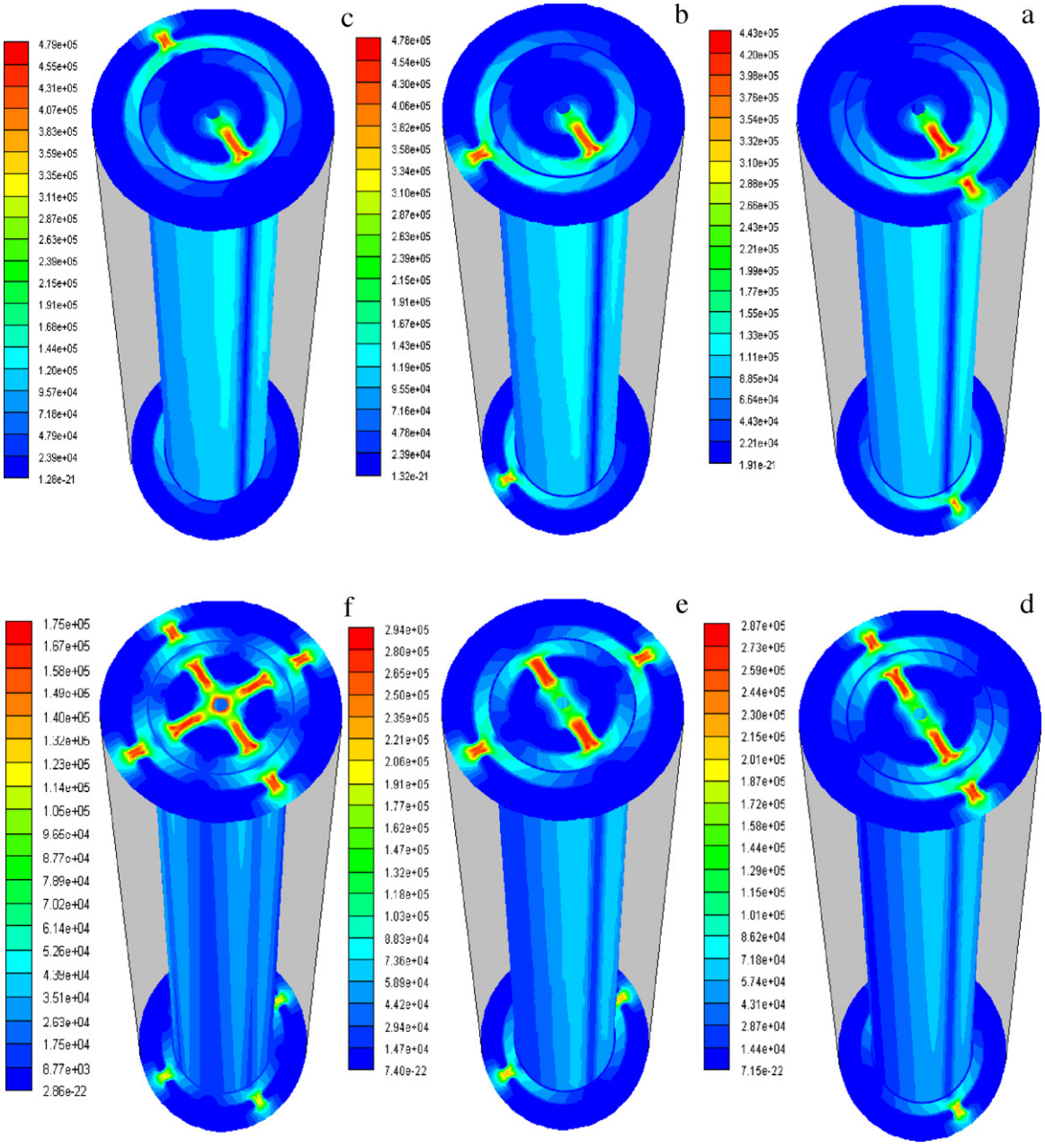

Fig. 6. Current density distribution at the cathode side catalyst layer for $V = 0.4$ V with (a) one connection (1), (b) one connection (2), (c) one connection (3), (d) two connection (1), (e) two connection (2) and (f) four connection.

magnitude of water molar fractions is higher at cathode catalyst layer than the anode catalyst layer and when the number of connections between GDL and bipolar plate increases that it is due to by increasing the number of connections, the chemical reaction at cathode catalyst layer enhances and the current density decreases. Also it is shown that for one connection conditions, water molar fraction is unsymmetrical but by increasing the number of connections, symmetrical condition of water mole fraction obtained.

Fig. 6 shows the local current density distribution at the cathode side catalyst layer at 0.4 V cell voltage for six different connections between GDL and bipolar plate. It is clear that the current density is higher at the connections between GDL and bipolar plate that these peak regions of the distribution of the local current density are caused by the transverse installation of the connections. This phenomena means that better cell performance is achieved around the connections. This is due to the fact that the fuel gas is blocked by the connections installed in the flow channel, and more fuel gas is forced into and passes through the gas diffusion layer, which enhances the chemical reaction at the catalyst surface. It can be seen that the current density distribution is uniform when the connections between GDL and bipolar plate increases. Also it is clear that the maximum of local current density decreased by increasing the number of connections. But the magnitude of current density is at lower value when the connections of anode and cathode sides are at similar direction due to the deduction of passing distance of the electrons.

4. Conclusion

A complete three-dimensional and single phase model for annular-shaped proton exchange membrane (PEM) fuel cell was used to investigate the effect of using different connections between bipolar plate and gas diffusion layer on the performances, current density, and temperature and gas concentration. The complete three-dimensional model for PEM fuel cells based on the two-fluid method was numerically solved with constant-temperature boundary condition at surfaces of anode and cathode current collectors. The results of this paper are in good agreement with experimental results of Miansari et al. [11]. The results show that the cell performance is increased as the number of connections between GDL and bipolar plate increases but for one connection conditions the effect of changing the location of connection on cell performance is negligibly small. The results show that the water mole fraction gradually increases along the cell and the maximum of it is near the connections between GDL and bipolar plate. Also the results show that when the number of connections between GDL and bipolar plate increase, consumption of hydrogen and oxygen and production of water increases. Also the results show a depression region in temperature distribution around the location of the connections between GDL and bipolar plate that this depression region is caused by increasing the traversed distance of gases on the surface, which decreases the temperature of them and the formation of more water vapor at this region and condensation of them.

References

[1] J. Larminie, A. Dicks, Fuel Cell System Explained, 2nd ed., Wiley, 2003.
[2] T. Berning, N. Djilali, J. Power Sources 124 (2003) 440–452.
[3] M.S. Chiang, H.S. Chu, J. Power Sources 160 (2006) 340–352.
[4] Z.H. Wang, C.Y. Wang, K.S. Chen, J. Power Sources 94 (2001) 40–50.
[5] J.K. Kuo, T.S. Yen, C.K. Chen, Energy Conver. Manage. 49 (2008) 2776–2787.
[6] J.S. Yi, T.V. Nguyen, J. Electrochem. Soc. 145 (1998) 1149–1159.
[7] U. Sukkee, C.Y. Wang, J. Power Sources 125 (2004) 40–51.
[8] T.A. Zawodzinski, M. Neeman, L.O. Sillerud, S. Gottesfeld, J. Phys. Chem. 95 (1991) 6040–6044.
[9] T.A. Zawodzinski, J. Davey, J. Valerio, S. Gottesfeld, Electrochim. Acta 40 (1995) 297–302.
[10] S. Motupally, A.J. Becker, J.W. Weidner, J. Electrochem. Soc. 147 (2000) 3171–3177.
[11] Me. Miansari, K. Sedighi, M. Amidpour, E. Alizadeh, Mo. Miansari, J. Power Sources 190 (2009) 356–361.